Chemical Engineering Communications
Publication details, including instructions for authors and subscription information:
http://www.tandfonline.com/loi/gcec20

BUOYANCY-DRIVEN MOTION OF DROPS AND BUBBLES IN A PERIODICALLY CONSTRICTED CAPILLARY

M. HEMMAT [a] & A. BORHAN [a]
[a] Department of Chemical Engineering , The Pennsylvania State University , University Park , PA , 16802
Published online: 03 May 2012.

To cite this article: M. HEMMAT & A. BORHAN (1996) BUOYANCY-DRIVEN MOTION OF DROPS AND BUBBLES IN A PERIODICALLY CONSTRICTED CAPILLARY, Chemical Engineering Communications, 148-150:1, 363-384, DOI: 10.1080/00986449608936525

To link to this article: http://dx.doi.org/10.1080/00986449608936525

Chem. Eng. Comm., 1996, Vols. 148–150, pp. 363–384
Reprints available directly from the publisher
Photocopying permitted by license only

BUOYANCY-DRIVEN MOTION OF DROPS AND BUBBLES IN A PERIODICALLY CONSTRICTED CAPILLARY

M. HEMMAT and A. BORHAN*

Department of Chemical Engineering, The Pennsylvania State University, University Park, PA 16802

(Received April 3, 1995; in final form November 1, 1995)

Buoyancy-driven motion of viscous drops and air bubbles through a vertical capillary with periodic constrictions is studied. Experimental measurements of the average rise velocity of buoyant drops are reported for a range of drop sizes in a variety of two-phase systems. The instantaneous drop shapes at various axial positions within the capillary are also quantitatively characterized using digital image analysis. Periodic corrugations of the capillary wall are found to have a substantial retarding effect on the mobility of drops in comparison with previous experimental results in a straight cylindrical capillary. For systems characterized by small Bond numbers, drop deformations are found to be periodic. In large Bond number systems, however, drop breakup eventually occurs as the drop size is increased beyond a critical limit. The observed mode of breakup is a tail-pinching process similar to that observed by Olbricht and Leal (1983) for pressure-driven motion of low viscosity ratio drops through a sinusoidally constricted capillary. In contrast to their results, however, the same mode of breakup was also observed for systems with $O(1)$ viscosity ratios.

KEYWORDS Buoyancy Drops Bubbles Constricted capillary

INTRODUCTION

The motion of drops and bubbles through capillaries of constant and variable cross-section remains of considerable fundamental importance as a pore-scale model for studying the dynamics of two-phase flow through porous media. Although a straight cylindrical capillary is a gross oversimplification of the true pore geometry in a porous material, it has served to identify the important parameters affecting the mobility of the dispersed phase in flow through porous media. An improved pore-scale model can be obtained by considering capillaries with variable cross-sectional area, in which Lagrangian unsteady motion of drops and bubbles can occur. In particular, a capillary whose cross-sectional area varies periodically in the axial direction presents an improvement over the straight cylindrical capillary model because of its inherent converging/diverging configuration that reproduces some of the essential features of the flow kinematics associated with flow through real pore spaces. Experimental observations of Olbricht and Leal (1983) indicate that a liquid drop forced through such a capillary by an imposed pressure-driven flow can experience substantial uniaxial extension and biaxial expansion.

* Author to whom correspondence should be addressed.

Previous studies of the motion of drops through capillaries have been mainly restricted to the case of straight cylindrical or polygonal capillaries with uniform cross-sectional areas, as summarized elsewhere (Olbricht, 1996; Borhan and Mao, 1992). Aside from a few exceptions (Martinez and Udell, 1989; Westborg and Hassager, 1989; Gauglitz and Radke, 1990; Borhan and Hemmat, 1992; Tsai and Miksis, 1994), theoretical investigations involving capillaries with nonuniform cross-section have been limited to single-phase flows (cf. Hemmat and Borhan, 1995). Oh and Slattery (1979) performed a static analysis to determine the critical value of the pressure drop which must be exceeded in order to displace a fluid globule in a sinusoidally constricted capillary, but did not examine the motion of the fluid particle. Westborg and Hassager (1989), and Tsai and Miksis (1994), analyzed the pressure-driven motion of a deformable viscous drop through a single constriction in a cylindrical capillary. Westborg and Hassager (1989) found that, for axisymmetric constrictions, drop breakup could only be initiated by a sudden decrease in the flow rate after the drop had protruded some distance beyond the throat, whereas, for nonaxisymmetric constrictions, drop breakup could occur during continuous operation. On the other hand, Tsai and Miksis (1994) reported the occurrence of breakup in continuous pressure-driven flow through an axisymmetric constriction for very low viscosity ratio drops. Martinez and Udell (1989) performed a computational study of the motion of neutrally-buoyant drops through sinusoidally constricted capillaries but did not report any drop breakup in the range of parameters considered.

On the experimental side, Goldsmith and Mason (1963) observed breakup in forcing large bubbles through a converging section formed by connecting two straight capillaries with different diameters. Similarly, Han and Funatsu (1976) studied drop deformation and breakup in pressure-driven flow through an abrupt contraction, while Chin and Han (1979, 1980) performed similar experiments in the conical entrance section to a cylindrical capillary. In all of these experiments, drop breakup was observed downstream of the constriction. In the context of this study, however, the most relevant experimental work has been performed by Olbricht and Leal (1983) who considered the pressure-driven motion of immiscible neutrally-buoyant drops (both Newtonian and viscoelastic) in pressure-driven flow through horizontal capillaries whose diameter varied periodically with the axial position. They measured the average drop speed through the capillary and the extra pressure loss due to the presence of the drop, and correlated those values with the observed time-dependent drop shapes. Although their results for drop deformation and breakup were mainly qualitative in nature, they demonstrated the profound effect of the capillary geometry on the shape and mobility of drops. In addition to periodic deformations of small drops, they observed gross elongations of larger drops leading to eventual breakup as they passed through consecutive constrictions.They reported two distinct modes of drop breakup for small and $O(1)$ viscosity ratio drops, respectively, and identified the extensional strength of the imposed flow as the underlying mechanism responsible for the breakup process.

In this study, we focus on the buoyancy-driven motion of viscous drops and gas bubbles through a vertical capillary with periodic corrugations in order to examine the role of capillary geometry on drop deformation and breakup. Experimental measurements of the average rise velocity of buoyant drops through the capillary, as well as the observed drop shapes, will be reported over a wide range of the governing parameters,

viz. the dimensionless drop size, κ, defined as the ratio of the equivalent spherical drop radius to the average capillary radius R, the ratio of the drop to suspending fluid viscosities, λ, the corresponding ratio of fluid densities, γ, and the Bond number, $Bo = \Delta\rho g R^2/\sigma$, representing the ratio of buoyancy to interfacial tension forces; $\Delta\rho$ and σ represent the density difference and interfacial tension between the drop and suspending fluid, respectively, and g is the gravitational acceleration. Drop deformations will be quantitatively examined using digital image analysis techniques in order to extract geometric information that may be used to correlate the measured drop speeds. In addition, it will be shown that in the absence of an imposed pressure-driven flow, another mechanism, namely the hydrodynamic interaction between the drop and the capillary wall, can lead to substantial elongations of drops and bubbles, as well as a mode of drop breakup which is similar to that observed by Olbricht and Leal (1983).

EXPERIMENTAL PROCEDURE

A sketch of the experimental apparatus is shown in Figure 1. It consisted of a vertical glass tube composed of a 30 cm long straight cylindrical entry section of internal

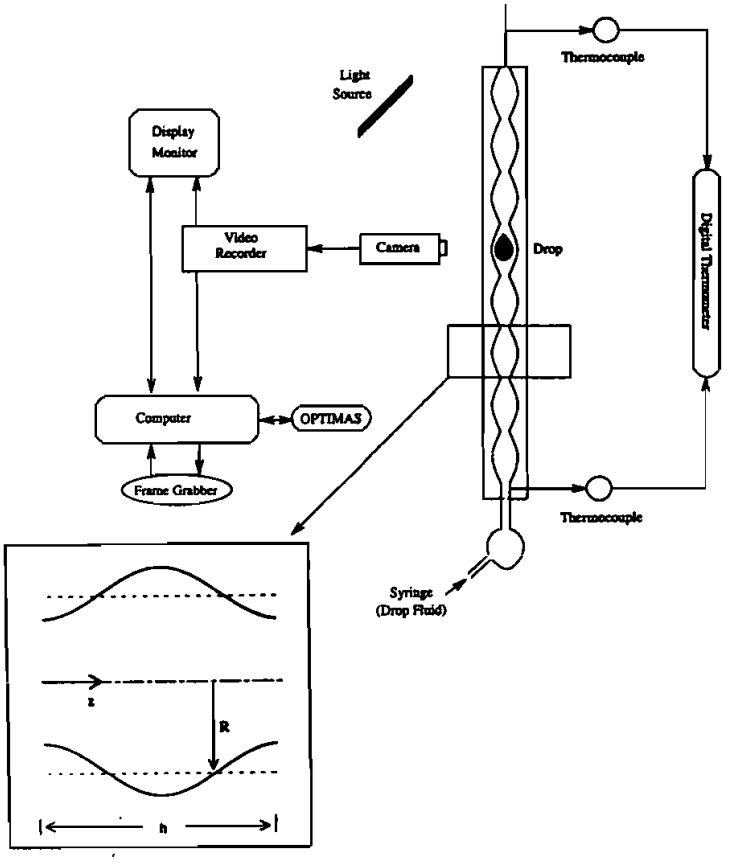

FIGURE 1 Schematic diagram of the experimental setup.

diameter 1.00 cm, followed by an 80 cm long periodically constricted test section. The test section included twenty identical sinusoidal corrugations with an average internal radius of 0.50 cm, wavelength of 4.00 cm, and amplitude of 0.07 cm. The suspending fluids used in the experiments were various aqueous glycerol solutions (denoted by GW and WG) and diethylene glycol-glycerol mixtures (denoted by DEG and DEGG). A variety of Ucon oils and Dow Corning fluids, silicon oil, and air were used as the drop phase. Experiments were performed with 14 different two-phase systems encompassing a wide range of material parameters, as shown in Table 1. In all cases, the density of the drop phase was lower than that of the suspending fluid. In order to facilitate the presentation of the experimental results, each two-phase system in Table 1 is labeled by a symbol identifying the suspending fluid, followed by a number specifying the drop fluid. All fluid properties shown in this Table were measured at a temperature of 25°C. Liquid viscosities were measured using capillary viscometers, while interfacial tensions were measured using a tensiometer which operates based on the principles of the Du Noüy ring and the Wilhelmy plate.

For each experiment, a known volume of the drop fluid was injected into the capillary using a microsyringe, and the motion of the drop through the capillary was recorded by a video camera equipped with macrolenses. The video camera was mounted on an elevator with variable speed control so as to allow the camera to move with the drop speed and monitor the drop as it passed through the entire length of the capillary. The motion of the drop through the capillary was recorded by a video recorder capable of frame by frame playback. To examine deformations of the drop shape at various locations within the capillary, recorded images of the drop profile (about 30 frames per second) were digitized using a computer equipped with a frame-grabber board. The Bioscan Optimas image analysis software was then used to quantitatively characterize the drop shapes. In order to minimize optical distortions of the drop shape caused by the curvature of the glass tube, the capillary was enclosed in a plexiglass chamber of square cross-section containing an aqueous sodium iodide solution with a refractive index equal to that of the glass tube. In addition, a stop motion filter was applied to the digitized images before image analysis in order to remove any jittering caused by the motion of the drop. Various geometric features of the drop shape, such as the perimeter and area of the drop profile and its maximum axial and equatorial dimensions, were measured as a function of the axial location of the drop within the capillary. Taking advantage of the axial symmetry of the drop shapes, the drop volume was also determined using Optimas to detect any inaccuracies in the drop size measurements based on the microsyringe reading.

The average rise velocity of the drop through one period of corrugation was determined by measuring the time required for the drop to travel a specified distance marked on the capillary wall. During each experiment, three independent velocity measurements over different corrugated regions of the capillary were made to check for variations in the average velocity. Furthermore, each experiment was repeated to ensure reproducibility of the results. In all cases, the reported average velocity represents the mean value from six independent velocity measurements. The variation of any single measurement from the reported mean value was less than 5% in all experiments.

TABLE 1
Two-phase systems used in the experiments

System	Suspending fluid	Drop fluid	Viscosity of suspending fluid (mPa.s)	Viscosity of drop fluid (mPa.s)	Density of suspending fluid (kg/m^3)	Density of drop fluid (kg/m^3)	Interfacial tension ($N/m \times 10^3$)
GW1	glycerol-water (96.2wt%)	silicon oil	450	238	1,250	967	24.0
GW3	glycerol-water (96.2wt%)	UCON-1145	450	530	1,250	995	10.5
GW4	glycerol-water (96.2wt%)	UCON-50HB55	450	83	1,250	970	3.0
GW5	glycerol-water (96.2wt%)	UCON-50HB100	450	97	1,250	950	5.7
GW6	glycerol-water (96.2wt%)	air	450	0	1,250	1.3	42.0
GW8	glycerol-water (96.2wt%)	DC510-500	450	607	1,250	993	25.0
WG1	glycerol-water (90.6wt%)	silicon oil	190	238	1,230	967	23.0
WG2	glycerol-water (84.3wt%)	DC510-100	83	104	1,220	990	25.7
WG4	glycerol-water (82.6wt%)	UCON-50HB55	67	83	1,200	970	1.9
WG8	glycerol-water (95.6wt%	DC510-500	434	607	1,240	993	25.0
DEG3	diethylene glycol (100.0wt%)	UCON-1145	28	530	1,110	995	3.2
DEG10	diethylene glycol (100.0wt%)	UCON-165	28	63	1,110	975	1.6
DEGG11	diethylene glycol-glycerol (63.8wt%)	UCON-385	87	157	1,160	968	5.0
DEGG12	diethylene glycol-glycerol (63.8wt%)	UCON-285	87	115	1,160	966	4.2

Note: All physical properties were measured at 25°C.

RESULTS AND DISCUSSION

We present the experimental results in terms of the effects of drop size, Bond number, and viscosity ratio on the shape and mobility of the drop. In all cases discussed here, drops and bubbles remained axisymmetric as they passed through the capillary. The periodic variations of the cross-sectional area of the capillary in the axial direction cause the velocity and shape of the drops to be position-dependent. We shall examine the instantaneous drop shapes at various axial positions within a period of corrugation, but limit the discussion of drop mobility to the average drop speed, U, over a period of corrugation. The values of the dimensionless parameters for each set of experiments with the same two-phase system are shown in Table 2. The range of measured average velocities for each system is also shown in the last column of this Table in the form of a capillary number defined as $Ca = \mu U/\sigma$. The Reynolds numbers ($Re = \rho UR/\mu$) encountered in all of these experiments were in the range of $5.0 \times 10^{-3} < Re < 3.0$.

We begin with a qualitative analysis of the shapes of drops and bubbles shown in Figures 2–6. A sequence of images for the evolution of the shape of a viscous drop as it moves through one period of corrugation is presented in Figure 2. When a large drop ($\kappa > 0.7$) reaches a constriction, its leading end follows the capillary wall contour and squeezes through the throat. Once the leading meniscus clears the throat, its rise speed increases as it enters the diverging cross-section, while the trailing end of the drop remains trapped behind the throat. This results in substantial extension of the drop in the axial direction and the formation of a narrow tail section. As the leading end advances beyond the throat, the curvature of the trailing end increases significantly while that of the leading meniscus remains nearly unchanged. The resulting capillary pressure difference between the trailing and leading ends of the drop leads to the acceleration of the fluid in the tail section as the trailing end leaves the constriction. This, combined with a notable reduction in the rise speed of the advancing meniscus as it enters the converging cross-section, causes the tail section to disappear, and the drop

TABLE 2
Range of dimensionless parameters

System	λ	γ	Bo	κ	Re $\times 10^3$	Ca $\times 10^3$
GW1	0.53	0.77	3.3	0.45–1.00	10–30	13–38
GW3	1.18	0.80	6.8	0.45–1.00	19–36	49–93
GW4	0.18	0.78	26.3	0.45–0.94	72–78	771–824
GW5	0.22	0.76	14.8	0.45–0.96	65–68	438–460
GW6	0.00	0.001	8.4	0.45–1.88	240–312	157–205
GW8	1.35	0.79	2.9	0.45–1.00	5–24	7–33
WG1	1.25	0.79	3.2	0.45–1.00	26–216	6–52
WG2	1.25	0.81	2.5	0.45–0.87	321–681	13–28
WG4	1.24	0.81	34.1	0.45–0.87	2274–2410	863–915
WG8	1.40	0.80	2.8	0.45–1.18	5–32	6–37
DEG3	18.86	0.90	10.1	0.45–1.46	1212–2312	51–97
DEG10	2.25	0.88	23.8	0.45–1.33	2558–2945	222–256
DEGG11	1.80	0.83	10.8	0.45–1.55	342–522	84–116
DEGG12	1.32	0.83	13.0	0.45–1.46	401–555	115–118

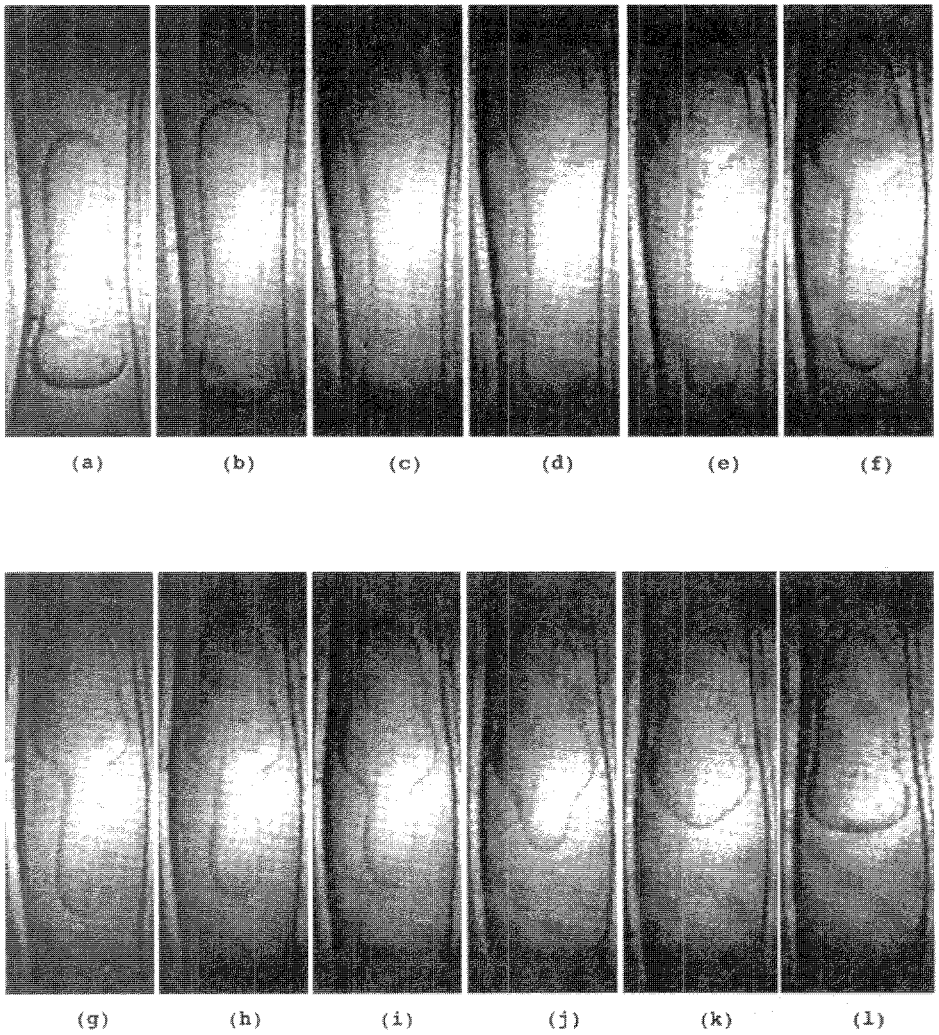

FIGURE 2 A viscous drop of size $\kappa = 1.07$ rising through a period of corrugation (DEGG11 system). The dimensionless time, $\tau = Ut/h$, for each image is given by; (*a*) 0.00, (*b*) 0.13, (*c*) 0.33, (*d*) 0.43, (*e*) 0.51, (*f*) 0.58, (*g*) 0.60, (*h*) 0.61, (*i*) 0.63, (*j*) 0.67, (*k*)0.70, (*l*) 0.73.

to assume its original shape. A qualitatively similar shape evolution is exhibited by large air bubbles moving through the capillary, as shown by the sequence of images in Figure 3. However, the air bubbles follow the wall contour more closely as they pass through the corrugations, forming a liquid film of nearly uniform thickness between the interface and the capillary wall.

The drop profiles in Figures 4–6 qualitatively demonstrate the sensitivity of the shape of viscous drops to the value of the Bond number, keeping other parameters nearly constant. Increasing the Bond number seems to produce more elongated drop

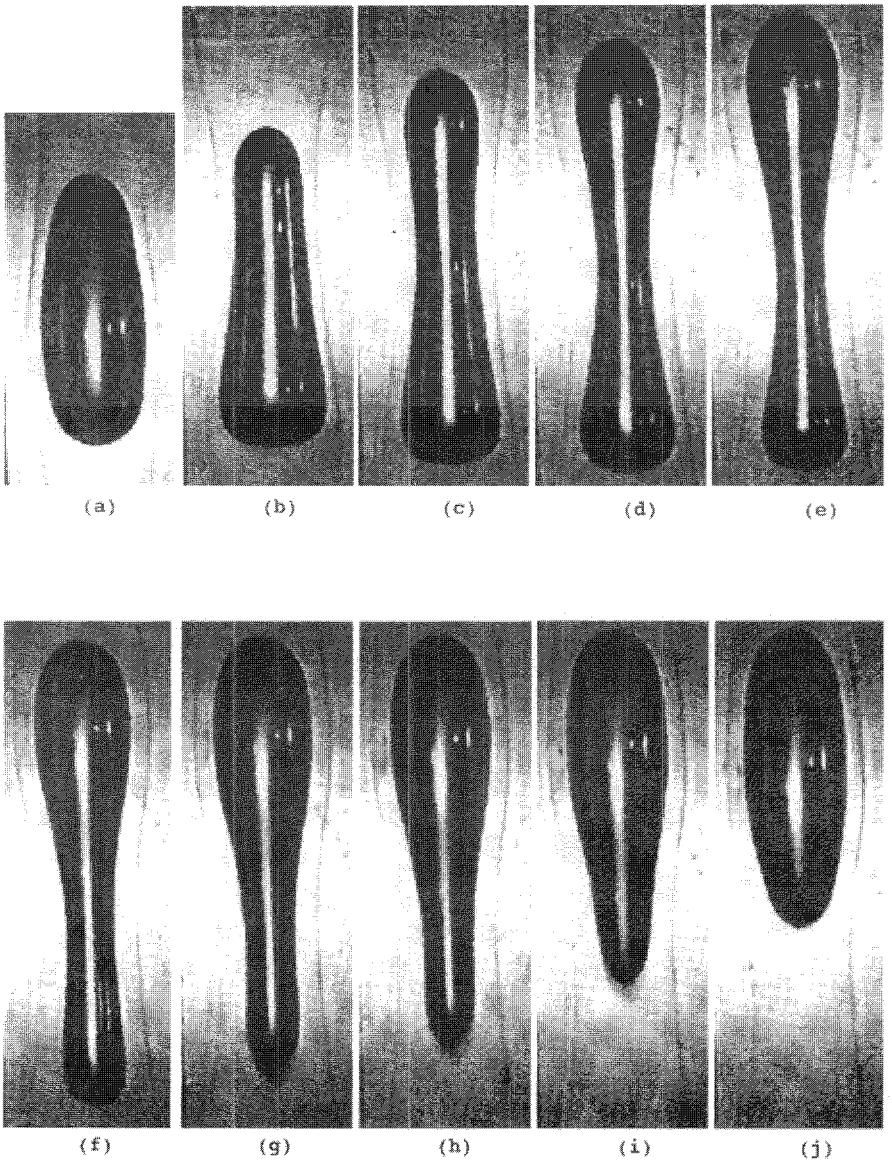

FIGURE 3 An air bubble of size $\kappa = 1.23$ rising through a period of corrugation (GW6 system). A dimensionless time, τ, for each image is given by; (*a*) 0.00, (*b*) 0.32, (*c*) 0.60, (*d*) 0.70, (*e*) 0.76, (*f*) 0.81, (*g*) 0.85, (*h*) 0.88, (*i*) 0.93, (*j*) 0.97.

shapes, particularly for larger drop sizes. In order to quantitatively characterize the evolving shapes of drops and bubbles as they pass through the corrugations, a deformation parameter D is defined as the ratio of the perimeter of the deformed drop profile to that of the equivalent spherical drop. This quantity is easily obtained from digitized

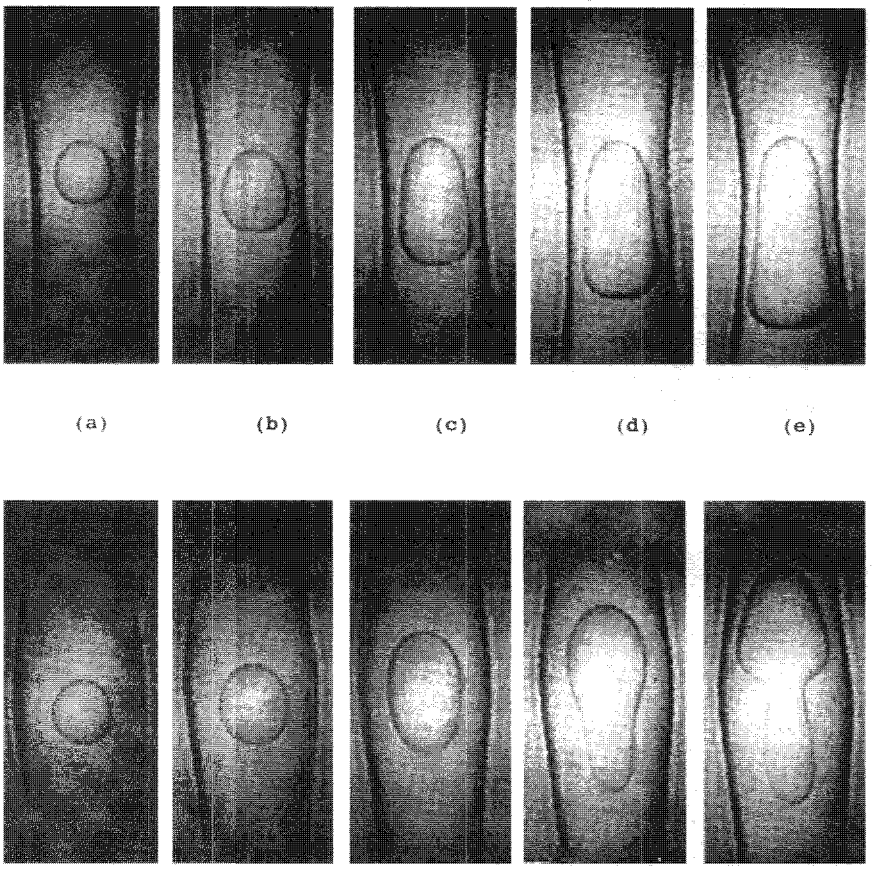

FIGURE 4 Comparison of the shapes of viscous drops in the throat and expansion regions of the capillary for the DEGG12 system ($Bo = 13.0$, $\lambda = 1.32$); (*a*) $\kappa = 0.54$, (*b*) $\kappa = 0.65$, (*c*) $\kappa = 0.78$, (*d*) $\kappa = 0.85$, (*e*) $\kappa = 0.92$.

images of drops and bubbles using the Optimas image analysis software. Figures 7–10 show the variations of the deformation parameter as a function of the axial position of the drop within one period of corrugation, for several drop sizes. The axial position, z, in these figures represents the axial distance between the tip of the drop and the preceding constriction, normalized by the wavelength of corrugation, h. Also shown in these figures is the axial length of the drop profile scaled by the wavelength of corrugation, denoted by L. The deformation parameter was found to be periodic for all drop sizes, except for the experiments in which drop breakup was observed.

As expected, increasing the drop size leads to larger deformations and more elongated drop shapes at all axial positions within the capillary. Whereas small drops are characterized by nearly constant values of D and L over a period of corrugation, large drops ($\kappa > 0.7$) exhibit significant variations in these parameters as a function of axial position. Furthermore, the fluctuations in the deformation parameter grow with

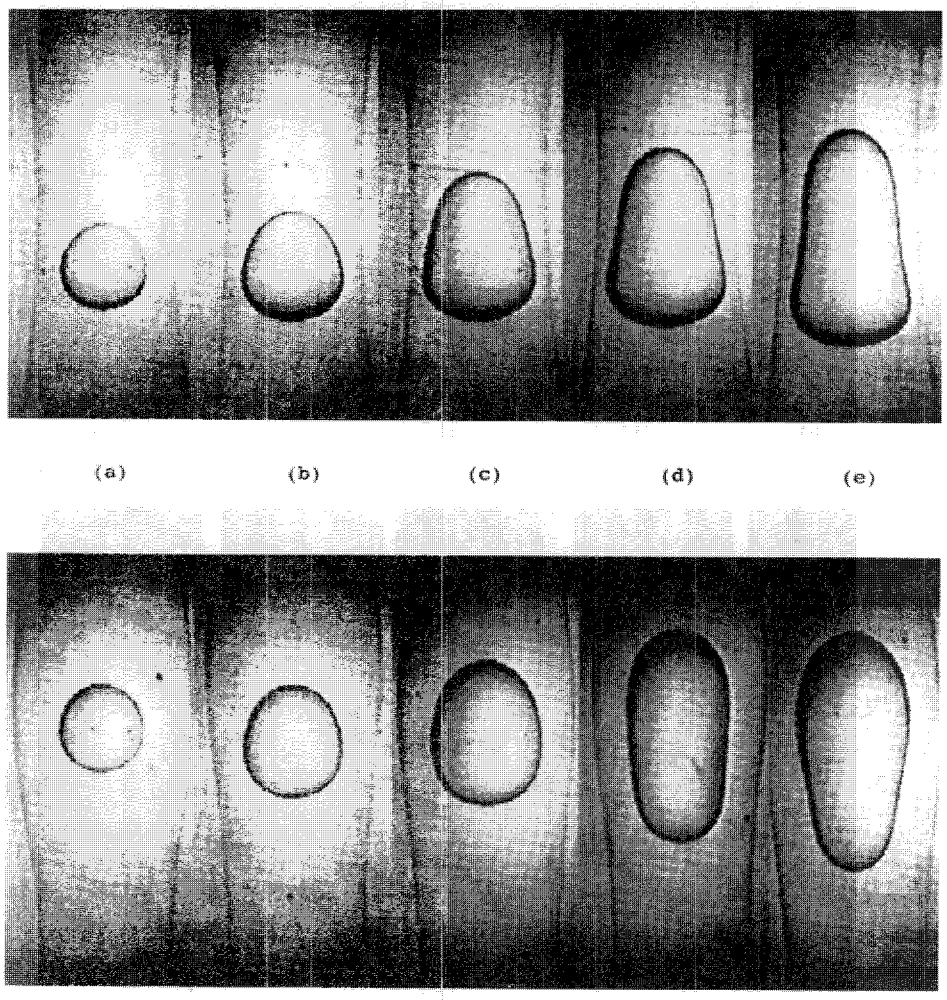

FIGURE 5 Comparison of the shapes of viscous drops in the throat and expansion regions of the capillary for the GW3 system ($Bo = 6.8$, $\lambda = 1.18$); (*a*) $\kappa = 0.54$, (*b*) $\kappa = 0.65$, (*c*) $\kappa = 0.78$, (*d*) $\kappa = 0.85$, (*e*) $\kappa = 0.92$.

increasing drop size until $\kappa > 1$, when the length of the drop becomes larger than the corrugation wavelength. It is clear from Figures 7–10 that, for $\kappa < 1$, the locus of the maxima in L approximately coincides with the dotted line $L = z$. This implies that such drops assume their most stretched configuration just before their trailing ends leave the throat. It is easy to verify that the maximum values of D also occur for the same drop configurations. For drops or bubbles larger than a corrugation wavelength, on the other hand, the maximum values of L and D are achieved just before the advancing front enters the converging cross-section (at $z \cong 0.75$) and begins to slow down. This observation can also be verified by examining the bubble shapes in Figure 3. Figure 11 shows the maximum values of D within one period of corrugation as a function of drop

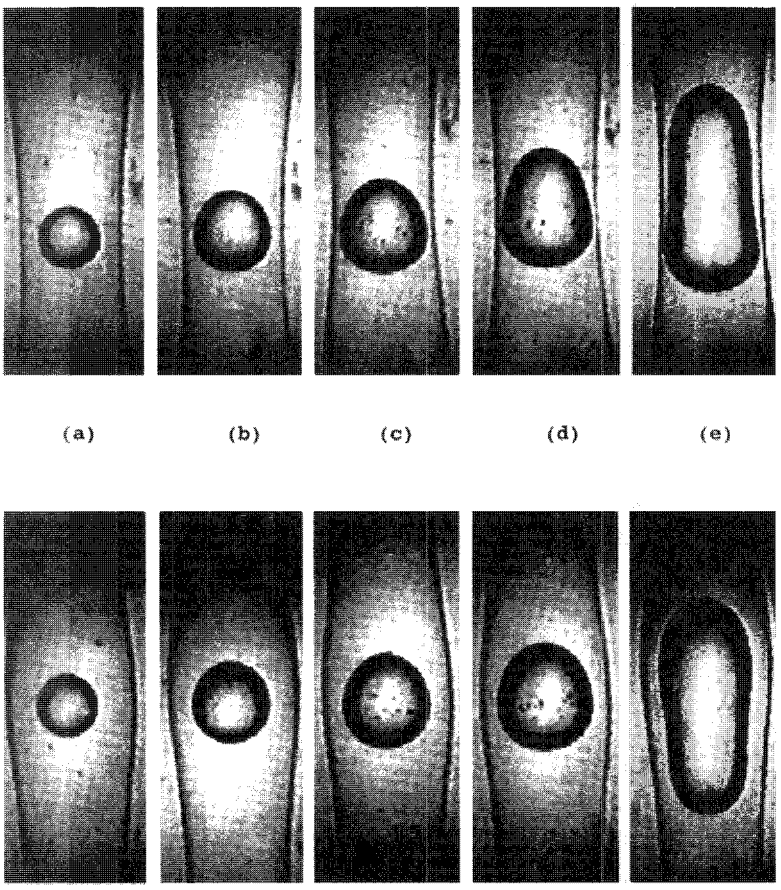

FIGURE 6 Comparison of the shapes of viscous drops in the throat and expansion regions of the capillary for the WG1 system ($Bo = 3.2$, $\lambda = 1.25$); (*a*) $\kappa = 0.54$, (*b*) $\kappa = 0.65$, (*c*) $\kappa = 0.78$, (*d*) $\kappa = 0.85$, (*e*) $\kappa = 1.02$.

size, for the experimental systems with different Bond numbers but nearly the same values of viscosity ratio. Clearly, increasing the Bond number leads to more elongated drop shapes as the drop passes through the constriction. A qualitatively similar trend with increasing viscosity ratio is demonstrated in Figure 12 for systems with approximately the same Bond number.

We now consider the effects of drop size, Bond number, and viscosity ratio on the average velocity of drops and bubbles rising through the periodically constricted capillary. The average velocities (made dimensionless with $\Delta\rho g R^2/\mu$ where μ is the viscosity of the suspending fluid) shown in Figure 13 demonstrate the two types of dependence on drop size observed in our experiments. For systems with small Bond numbers, a local maximum in the average rise velocity is reached for small drop sizes (at $\kappa \cong 0.5$) as the retarding effect of the capillary wall begins to overwhelm the increase in the buoyancy force with increasing drop size. In contrast, the local peak in the average

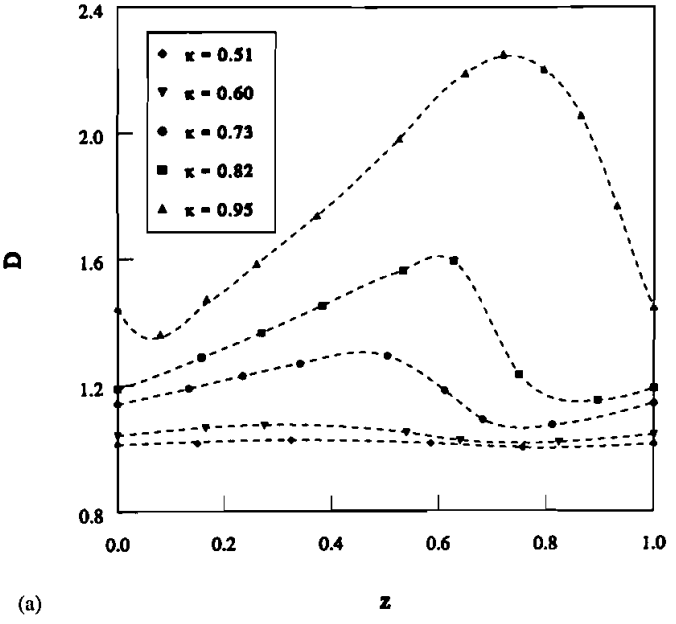

(a)

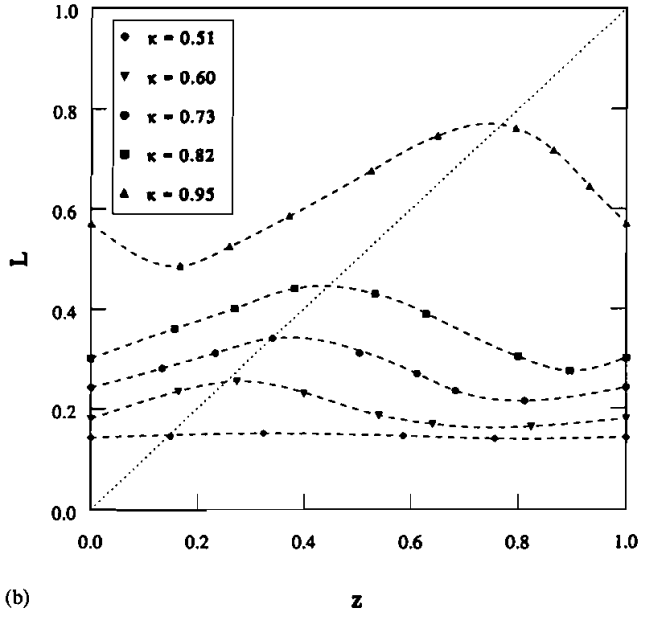

(b)

FIGURE 7 Variations of the geometric parameters with axial position of the advancing meniscus within one period of corrugation for the DEGG12 system ($Bo = 13.0$, $\lambda = 1.32$); (*a*) deformation parameter D, (*b*) drop length L. The dashed curves represent cubic spline fits to the experimental data.

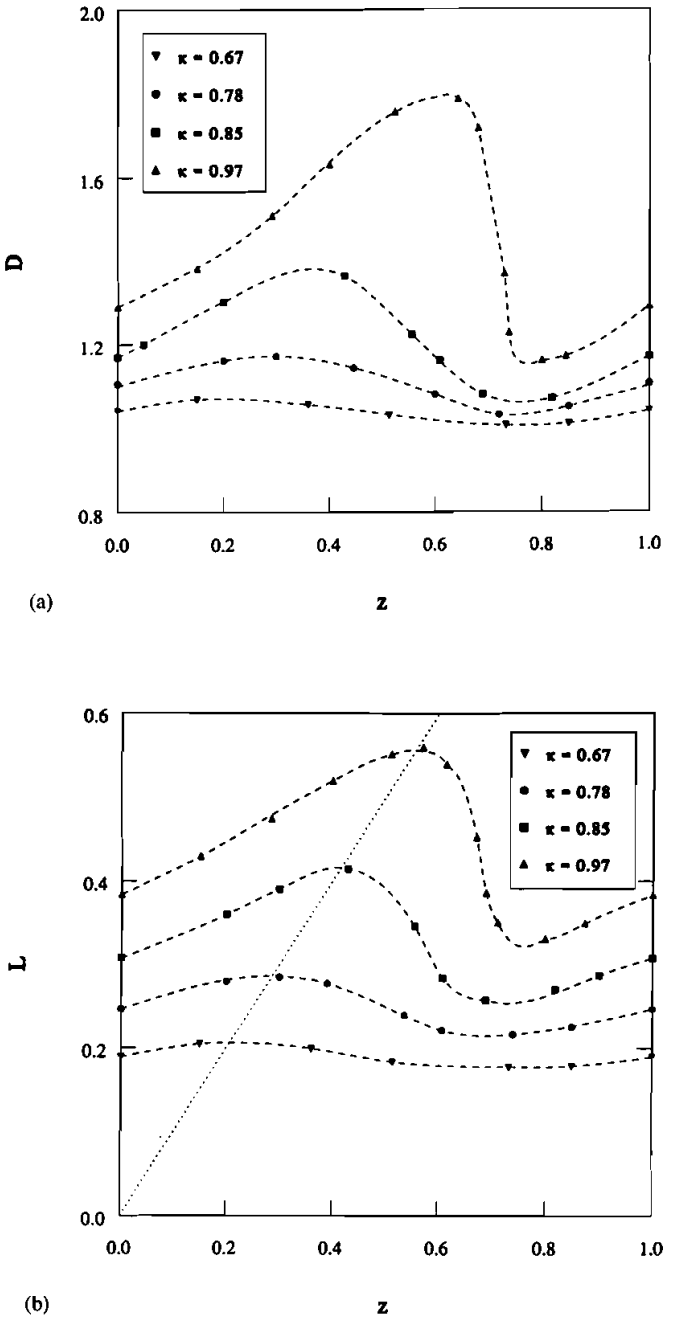

FIGURE 8 Variations of the geometric parameters with axial position of the advancing meniscus within one period of corrugation for the GW3 system ($Bo = 6.8$, $\lambda = 1.18$); (*a*) deformation parameter D, (*b*) drop length L.The dashed curves represent cubic spline fits to the experimental data.

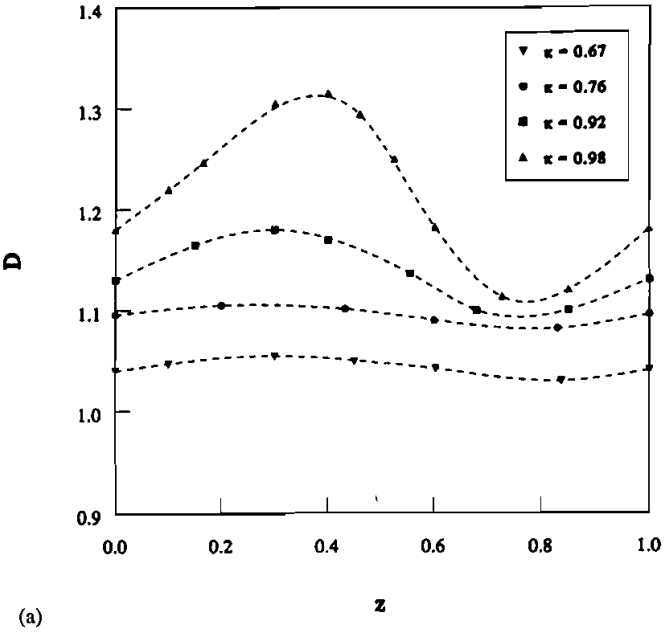

(a)

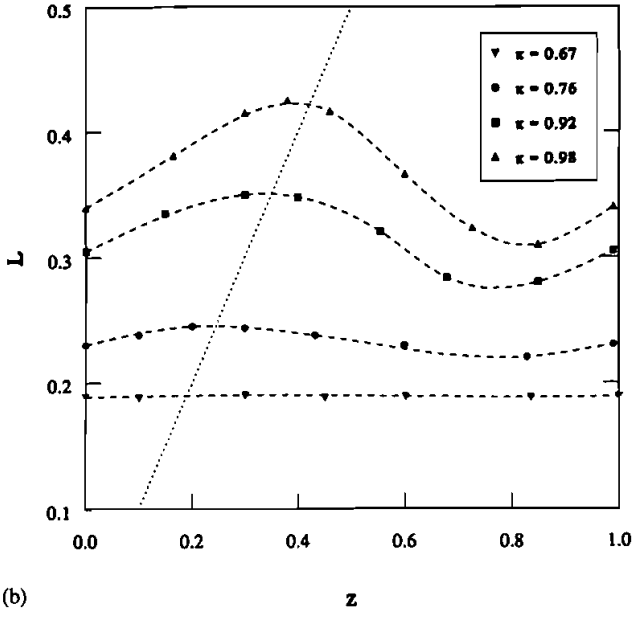

(b)

FIGURE 9 Variations of the geometric parameters with axial position of the advancing meniscus within one period of corrugation for the GW8 system ($Bo = 2.9$, $\lambda = 1.35$); (*a*) deformation parameter D, (*b*) drop length L. The dashed curves represent cubic spline fits to the experimental data.

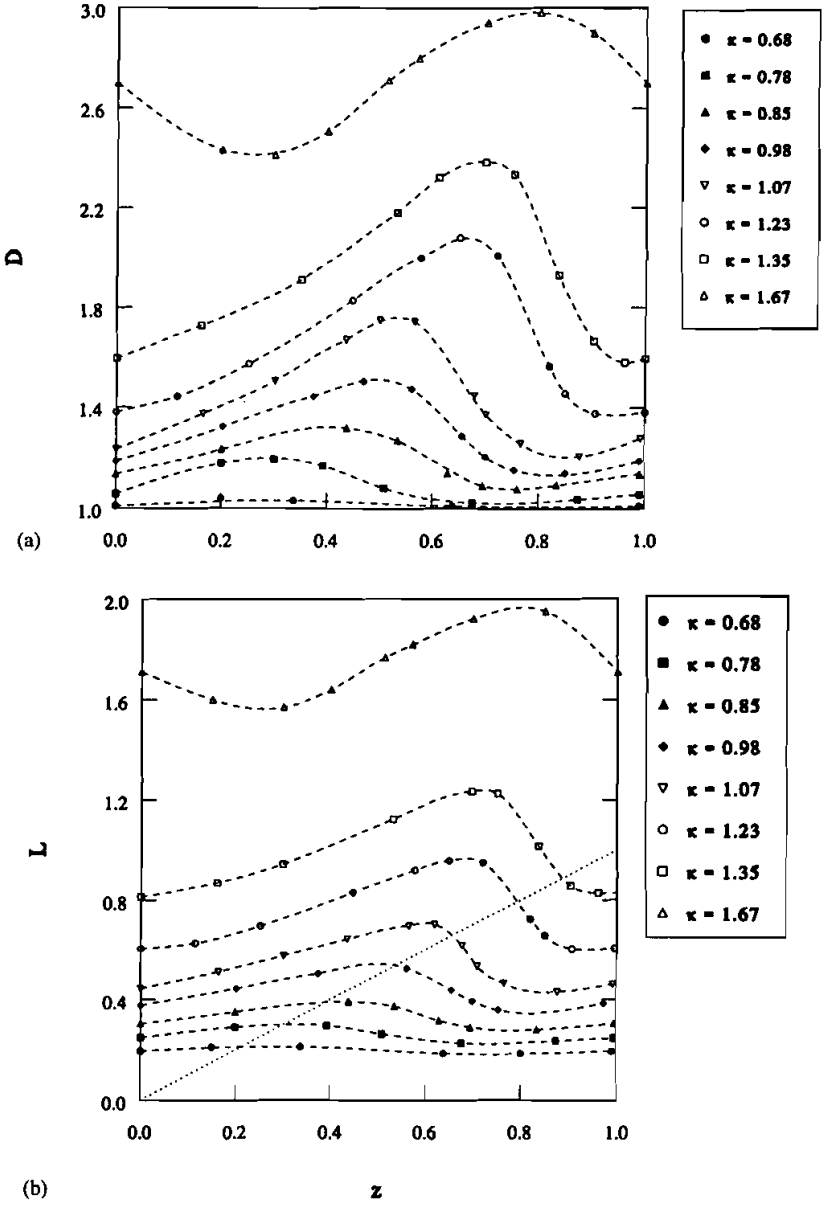

FIGURE 10 Variations of the geometric parameters with axial position of the advancing meniscus within one period of corrugation for the GW6 system ($Bo = 8.4$, $\lambda = 0.00$); (*a*) deformation parameter D, (*b*) bubble length L. The dashed curves represent cubic spline fits to the experimental data.

rise velocity seems to disappear in large Bond number systems. This difference can be attributed to the enhanced deformability of large drops at higher Bond numbers particularly as they squeeze through the throat. For a given drop size, the more elongated drop shapes formed at higher Bond numbers lead to thicker films of the

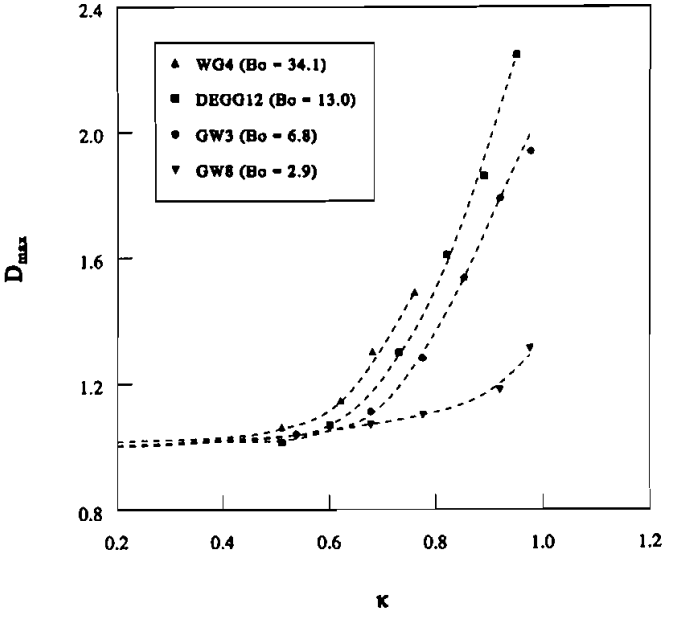

FIGURE 11 The effect of Bond number on the maximum deformation for systems with $\lambda \cong 1.2$–1.3. The dashed curves represent best visual fits to the experimental data.

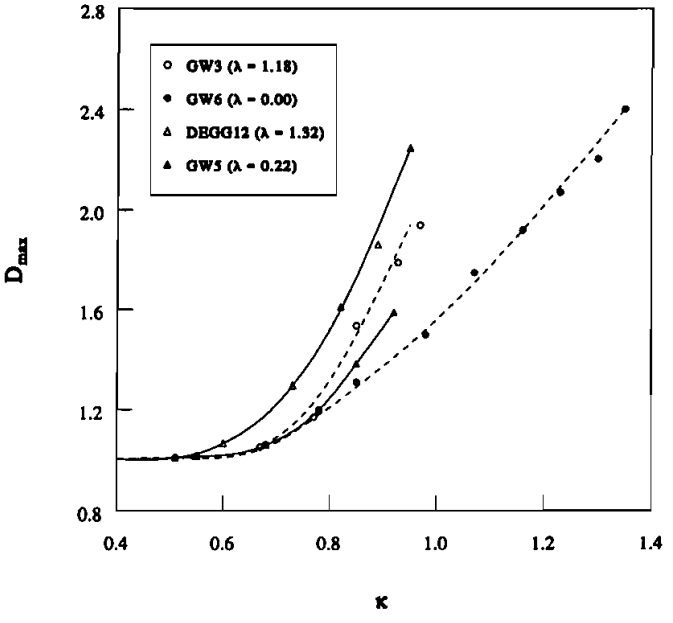

FIGURE 12 The effect of viscosity ratio on the maximum deformation for systems with nearly the same Bond number; (○, ●) $Bo \cong 7$–8; (△, ▲) $Bo \cong 13$–15. All curves represent best visual fits to the experimental data.

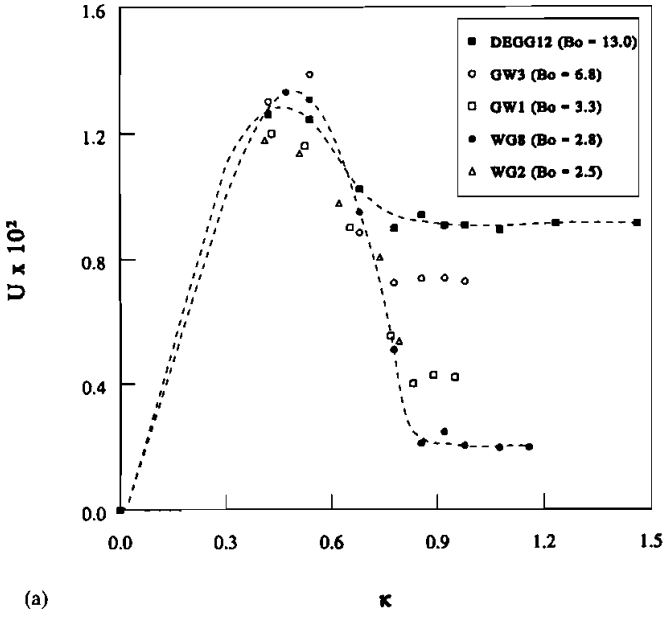

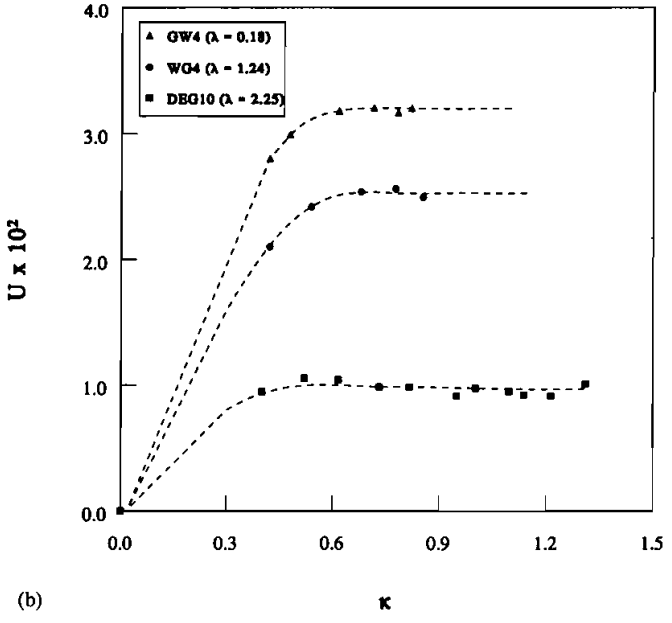

FIGURE 13 Dimensionless average rise velocity as a function of drop size; a) systems with $Bo < 15$, b) systems with $Bo > 15$. The dashed curves represent best visual fits to the experimental data.

suspending fluid between the drop and the capillary wall, thereby resulting in less drag on the drop for the same buoyancy driving force. In all cases, the average rise velocity eventually approaches a limiting value which remains unchanged with further increases in the drop size. These trends are qualitatively similar to those observed by Borhan and Pallinti (1995) for the buoyancy-driven motion of viscous drops through straight cylindrical capillaries.

In order to examine the retarding effect of the capillary wall on the motion of drops and bubbles, the average drop speed relative to U_∞, the rise velocity of an equivalent spherical drop of the same fluid in an infinite reservoir of the suspending fluid, is shown in Figures 14–15. As expected, the scaled average velocities are monotonically decreasing functions of drop size due to the drag exerted on the drops by the capillary wall. The open symbols in Figure 14 represent the experimental measurements of Borhan and Pallinti (1995) in a straight cylindrical capillary for a system that is characterized by approximately the same values of the dimensionless parameters as those for the GW3 system. A direct comparison between their measured drop mobilities and those for the GW3 system, shown in this figure, clearly demonstrates the substantial retarding effect of the periodic corrugations. The small amplitude corrugations of the capillary used in this study have led to more than a 50% reduction in the relative mobility of drops compared to the corresponding values in a straight cylindrical capillary. Figure 14 also shows an increase in the relative mobility of drops as the Bond number becomes larger. This is due to the enhanced deformability of drops at larger Bond numbers, which allows them to squeeze through the throat more easily. Figure 15 reveals the retarding

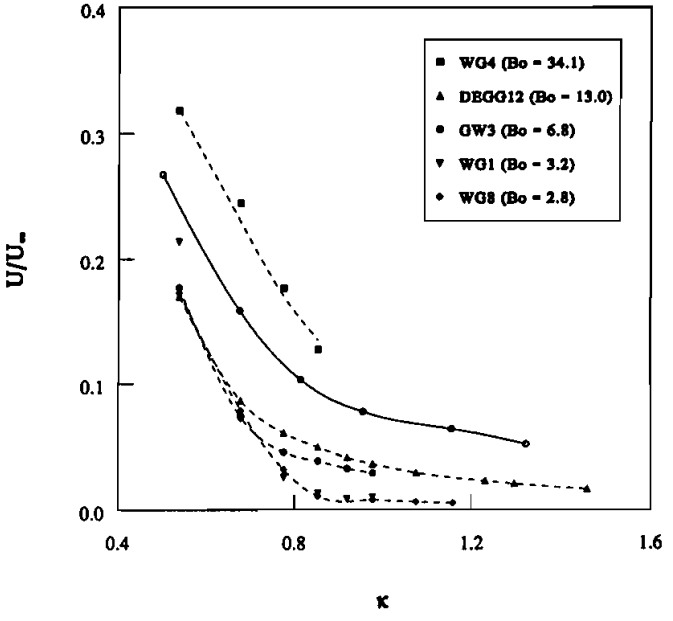

FIGURE 14 The effect of Bond number on the relative mobility of drops for systems with $\lambda \cong 1.2$–1.3. The open symbols represent the experimental data of Borhan and Pallinti (1995) for their WG5-1 system in a straight cylindrical capillary. All curves represent best visual fits to the experimental data.

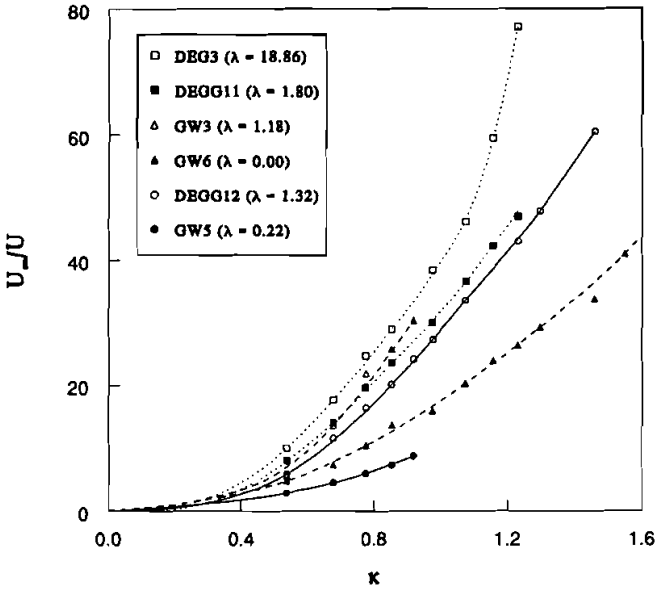

FIGURE 15 The effect of viscosity ratio on the retarding influence of the capillary wall for systems with nearly the same Bond number; (□, ■) $Bo \cong 10$–11, (△, ▲) $Bo \cong 7$–8, and (○, ●) $Bo \cong 13$–15. All curves represent best visual fits to the experimental data.

effect of larger viscosity ratios which cause the surface of the drop to become more rigid. The velocity measurements in this figure are presented in terms of U_∞/U to provide a better resolution of the experimental data since the values of U/U_∞ were quite small. Note that the variations of the average velocity with viscosity ratio in Figure 15 are entirely due to interactions of the drop with the capillary wall since the effect of viscosity ratio on the mobility of the drop in an infinite reservoir has already been removed through the choice of the velocity scale. According to this figure, the influence of the viscosity ratio (at fixed Bond number) on the relative mobility of drops seems to be more pronounced when the viscosity ratio is in the range $0 \leqslant \lambda \leqslant 1.5$.

The experimental data presented so far have been associated with the periodic motion and deformation of drops and bubbles in the periodically constricted capillary. For many systems in Table 1, however, increasing the drop size eventually led to drop breakup through a tail-pinching mechanism shown in Figure 16. For such systems, as a large drop moved through the constriction, the trailing end remained within the throat long enough to cause thinning of the midsection of the drop, followed by eventual pinch-off and formation of a satellite drop. One satellite drop was thus formed in each constriction as the drop passed through the capillary, until the drop became smaller than the critical drop size for the onset of drop breakup in that system. this mode of drop breakup, which was typically observed in systems characterized by large Bond numbers, is similar to that observed by Olbricht and Leal (1983) for pressure-driven motion of low viscosity-ratio drops through a sinusoidally constricted capillary.

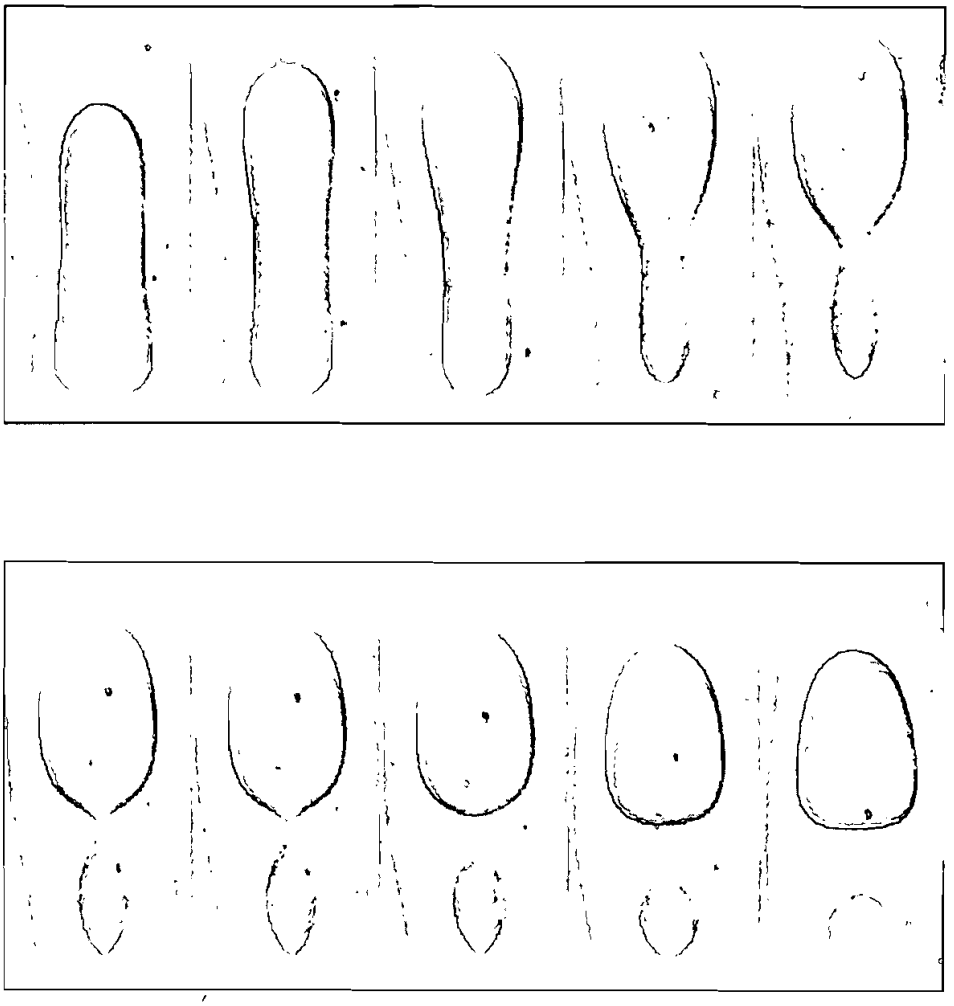

FIGURE 16 Breakup of a low viscosity ratio drop (GW5 system) as it passed through the constriction.

However, they observed a completely different mode of breakup for systems with $\lambda \sim O(1)$, whereas, in these experiments, the same mode of breakup was observed in all cases, including systems with $O(1)$ viscosity ratios (see Fig. 17). Olbricht and Leal attributed the observed breakup of drops in their experiments to the extensional strength of the imposed flow. Observations of a similar mode of breakup in the absence of imposed flow in our experiments suggest that the hydrodynamic interaction between the drop and the capillary wall can play an equally significant role in the deformation and breakup process. The latter mechanism might even provide an alternate explanation for the different deformation and breakup characteristics of eccentrically-positioned drops, compared to their concentric counterparts, in the experiments of

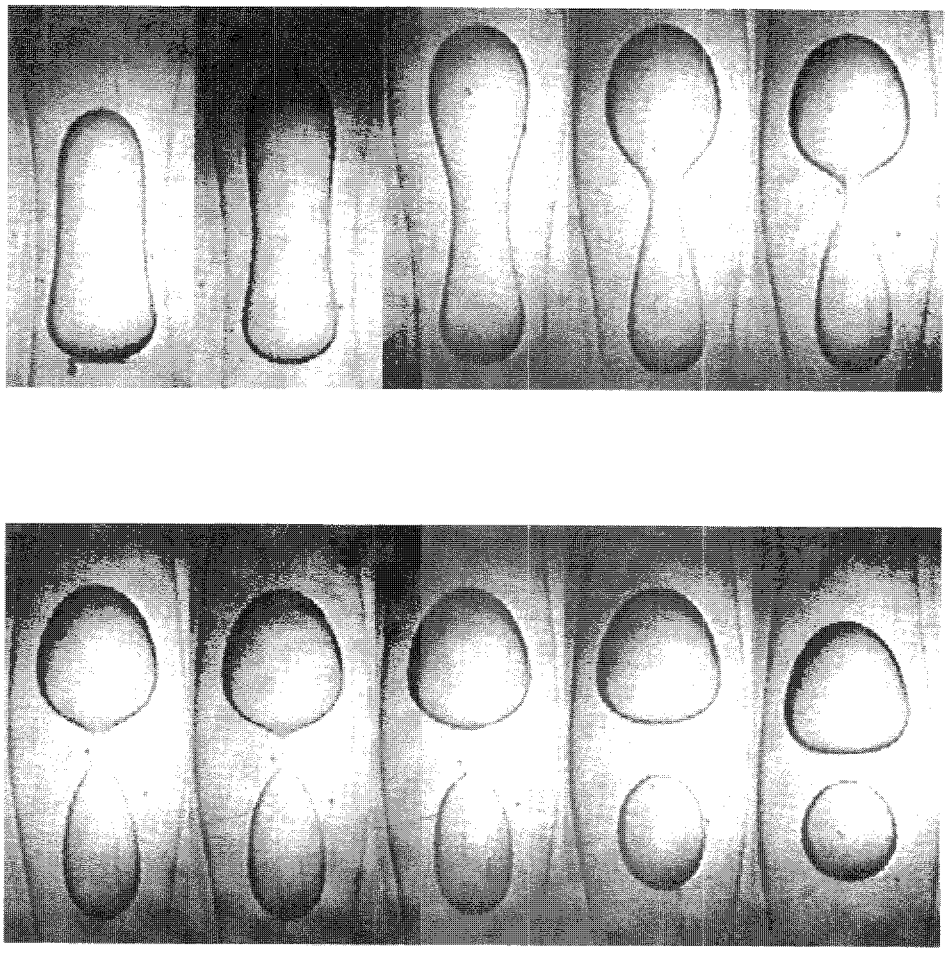

FIGURE 17 Breakup of a viscous drop as it passes through the constriction in a system with $O(1)$ viscosity ratio (WG4 system).

Olbricht and Leal. The role of the capillary geometry in determining the critical conditions for the onset of drop breakup warrants further investigation.

ACKNOWLEDGEMENT

Acknowledgment is made to the Donors of the Petroleum Research Fund, administered by the American Chemical Society, for partial support of this research.

REFERENCES

1. Borhan, A., and Hemmat, M., Creeping Motion of Drops through Periodically Corrugated Capillaries, *AIChE Annual Meeting, Miami Beach, FL*, (1992).

2. Borhan, A., and Mao, C. F., Effect of Surfactants on the Motion of Drops through Circular Tubes, *Phys. Fluids A*, **4**, 2628–2640 (1992).
3. Borhan, A., and Pallinti, J., Buoyancy-Driven Motion of Viscous Drops through Cylindrical Capillaries at Small Reynolds Numbers, *Ind. Eng. Chem. Res.*, **34**, 2750–2761 (1995).
4. Chin, H.B., and Han, C.D., Studies on Droplet Deformation and Breakup: I. Droplet Deformation in Extensional Flow, *J. Rheol.*, **23**, 557–590 (1979).
5. Chin, H.B., and Han, C.D., Studies on Droplet Deformation and Breakup: II. Breakup of a Droplet in Nonuniform Shear Flow, *J. Rheol.*, **24**, 1–37 (1980).
6. Gauglitz, P.A., and Radke, C.J., The Dynamics of Liquid Film Breakup in Constricted Cylindrical Capillaries, *J. Colloid Interface Sci.*, **134**, 14–40 (1990).
7. Goldsmith, H.L., and Mason, S.G., The Flow of Suspensions through Tubes: II. Single Large Bubbles, *J. Colloid Interface Sci.*, **18**, 237–261 (1963).
8. Han, C.D., and Funatsu, K., An Experimental Study of Droplet Deformation and Breakup in Pressure-Driven Flows through Converging and Uniform Channels, *J. Rheol.*, **22**, 113–133 (1976).
9. Hemmat, M., and Borhan, A., Creeping Flow through Sinusoidally Constriced Capillaries, *Phys. Fluids*, **7**, 2111–2121 (1995).
10. Martinez, M.J., and Udell, K. S., Axisymmetric Creeping Motion of Drops through a Periodically Constricted Tube, *AIP Conf. Proc.*, **197**, 222–234 (1989).
11. Oh, S.G., and Slattery, J.C., Interfacial Tension Required for Significant Displacement of Residual Oil, *Soc. Pet. Eng. J.*, **19**, 83–96 (1979).
12. Olbricht, W.L., Pore-Scale Prototypes of Multiphase Flow in Porous Media, *Ann. Rev. Fluid Mech.*, **28**, 187–214 (1996).
13. Olbricht, W.L., and Leal, L. G., The Creeping Motion of Immiscible Drops Through a Converging/Diverging Tube, *J. Fluid Mech.*, **134**, 329–355 (1983).
14. Tsai, T.M., and Miksis, M.J., Dynamics of a Drop in a Constricted Capillary Tube, *J. Fluid Mech.*, **274**, 197–217 (1994).
15. Westborg, H., and Hassager, O., Creeping Motion of Long Bubbles and Drops in Capillary Tubes, *J. Colloid Interface Sci.*, **133**, 135–147 (1989).